How is the relative impact of nudging and online coupling on meteorological variables, pollutant concentrations and aerosol optical properties?

Laurent MENUT[1], Bertrand BESSAGNET[1,2], Arineh CHOLAKIAN[1], Guillaume SIOUR[3], Sylvain MAILLER[1,4], and Romain PENNEL[1]

[1]Laboratoire de Météorologie Dynamique (LMD), Ecole Polytechnique, Institut Polytechnique de Paris, ENS, PSL Research University, Sorbonne Université, CNRS, Palaiseau, France
[2]Now at Joint Research Centre, European Commission, Ispra, Italy
[3]Univ Paris Est Créteil and Université Paris Cité, CNRS, LISA, 94010 Créteil, France
[4]Ecole des Ponts-ParisTech, Marne-la-Vallée, France

Correspondence: Laurent Menut, menut@lmd.ipsl.fr

Abstract.

Meteorological and chemical modelling at the regional scale often involve nudging of modeled meteorology towards reanalysis fields and meteo-chemical coupling to properly consider the interactions between aerosols, clouds and radiation. Both types of processes can change meteorology, but not for the same reasons and not necessarily in the same way. To assess the possible interactions between nudging and online coupling, several simulations are carried out with the WRF-CHIMERE model in its offline and online configuration. By comparison with measurements, we show that the use of nudging significantly improves the model performances. We also show that coupling changes the results much less than nudging. Finally, we show that when nudging is used, it limits the variability in the results due to coupling.

1 Introduction

The regional modelling of atmospheric pollution includes the modelling of meteorology and chemistry-transport. If the chemistry transport model (CTM) receives information from the meteorological model but does not send it back, it is an offline modeling. If, on the other hand, the two models exchange information, we are in an online modelling mode. Being regional, the models need forcing at the boundaries of the domain (lateral and top) and inside the domain. For the meteorological part and inside the domain, the technique used is called nudging and it could be 'grid' or 'spectral', (von Storch and Zwiers, 2001), (Kruse et al., 2022). With the spectral nudging, the meteorology can evolve due to mesoscale turbulence, but large-scale atmospheric circulations remain consistent with the global modelling that serves as forcing. Knowing that the global model has been corrected by data assimilation, the meteorological fields already implicitly contain the effects of aerosols on meteorology, Figure 1.

On the other hand, for chemistry-transport modeling (CTM) in online mode (increasingly used today and corresponding to the direct and indirect effects of aerosols on meteorology), aerosols will modify the meteorology within the simulation

domain. These changes are performed at higher spatial and temporal scales than the global forcing which is intrinsically a large scale process. Above all, they are completely independent of the large-scale circulation. It is therefore possible to have a contradiction between the scales: aerosols will modify the meteorology on the small scale, while at the same time, nudging will constrain the large scale to remain close to the initial global forcing.

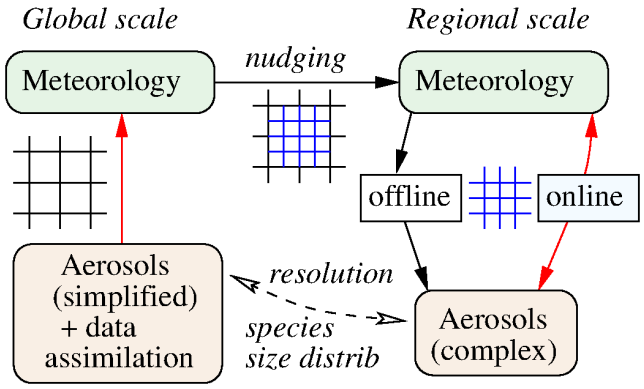

Figure 1. *The paradox of the regional model nudged by a global model. The global model performs a meteorological simulation, generally including aerosol climatology to take into account the direct and indirect effects of aerosols. If the simulation is a reanalysis, there may also be data assimilation, such as optical thickness estimated from satellite observations. But the overall simulation will have included aerosols in the meteorological calculation. This global simulation will serve as a forcing for the regional simulation. The regional meteorological model will serve as a forcing tool, or will be coupled to the chemistry-transport model calculating aerosols. Aerosols are also taken into account, but at a different resolution. The black grid is the global model and the blue grid the regional model. The dotted arrow indicates that aerosols may not be the same species or have the same size distribution, depending on the chemistry-transport and climatology models used.*

The effect of nudging on the modelling of regional meteorology is paradoxical: nudging improves the realism of simulations by forcing them to stay close to the observed reality, but this is achieved by introducing unrealistic inconsistencies between the dynamics and the physics of the model, therefore possibly limiting or distorting, (Lin et al., 2016), our understanding of processes by dampening the effect of model parameterizations. As presented in Figure 1, the global scale (used for nudging) and the regional scale are supposed to represent the same physical reality, but they rely on different aerosol forcings, spatial resolutions and parameterizations, therefore leading to divergent meteorology for the same location. We therefore have two processes acting in parallel: data assimilation on large-scale fields (global forcing, for example) and meteorological and chemical-transport coupling at a smaller scale. This paradox leaves the modeller with a methodological alternative. Either avoid nudging and let model physics operate freely, ensuring consistency between the physics and the dynamics, or use nudging and ensure that the model stays close enough to observations, but at the cost of introducing inconsistencies between the dynamics and the physics.

This methodological alternative has already been reported in regional and global climate modelling, particularly discussing the good use of nudging to evaluate model sensitivity to a forcing or to parameterization choices. It is already well-known in that

field that the use of nudging techniques, while indispensable for the representation of individual events in a realistic way, can dampen the response of models to other effects such as air-sea coupling (Berthou et al., 2016) or convective parameterizations, (Song et al., 2011). While improving the representation of individual events, nudging forces a model to reproduce a large-scale variability not necessarily in equilibrium with its physical parameterizations, thereby introducing inconsistency between the dynamics and physics, (Pohl and Crétat, 2013). On the bright side, nudging reduces the internal variability in the model, and therefore the spread between several different realizations, such as the sensitivity studies performed to evaluate the effect of a particular process or parameterization, permitting robust detection of such effects from shorter simulations, (Sun et al., 2019). For example, Kooperman et al. (2012) shows that, by attenuating the 'natural variability' between two sensitivity simulations, nudging permits to isolate the direct effect of a physical process from natural variability. In summary, the effect of nudging on sensitivity studies is twofold. On the one hand, it dampens the effect of a change in processes or parameterizations (Song et al., 2011; Pohl and Crétat, 2013; Lin et al., 2016; Berthou et al., 2016) and introduces inconsistencies between the dynamics and the physics (Pohl and Crétat, 2013; Lin et al., 2016), but on the other hand it strongly reduces the internal (chaotic) variability of meteorology in the numerical simulations, and thereby permits to observe sensitivity effects in a more robust way (Kooperman et al., 2012; Lin et al., 2016; Sun et al., 2019), even in relatively short simulations as it will be the case in the present study.

The effect of nudging on regional simulation has been studied mainly on meteorological variables such as temperature and precipitation. Using the WRF model (Powers et al., 2017), Glisan et al. (2013) studied the effect of the nudging on arctic temperature and precipitation. They showed that the strength of the nudging is not a sensitive key for the results. Spero et al. (2014) proposed changes in the spectral nudging to improve clouds, radiation and precipitation in their WRF simulations. The study of (He et al., 2017) is on climatological time-scale and more specifically on the possible changes in temperature due to the combined effects of large-scale forcing and regional aerosol/radiation interactions. They concluded that the use of nudging is possible and realistic for aerosol radiative effect studies, but with caution, the smaller the spatial scale. Rizza et al. (2020) explored the sensitivity of the WRF model to various configurations, including the spectral nudging. They compared their results to meteorological (wind, temperature) surface measurements and conclude there is no interest to nudge the meteorology inside the boundary layer.

For the impact of this methodology on pollutant concentrations, the focus of the present study, the studies are very rare. In these cases, they are more dedicated to regional climate (trends, long term scenarios) than to regional atmospheric pollution cases. One of the first study is (Hogrefe et al., 2015) which performed simulations tests in the framework of the AQMEII2 project and showed that the nudging reduces the bias for temperature with or without aerosol effects. They showed that, on temperature, the effect of the nudging is larger than the effect of the feedback of aerosols on meteorology. The same question arises in (He et al., 2017) about the relative impact of temperature nudging compared to aerosol radiative effects. They showed that the nudging has less effect than the aerosol-radiation interactions at global and regional scale, but could be more important at the local scale.

In the present study we will focus on regional scale modelling and spectral nudging impact both on meteorology and pollutant concentrations for a limited temporal scale. Simulations of the same case are carried out to evaluate the weight of nudging on cloud/radiative/aerosol interactions. The key question here is to know on a regional scale what is most important for pollutant

concentrations between nudging and coupling and how they interact. Even if they are not the same kind of processes and not directly comparable, they are often 'free parameters' up to the user, making it important to well understand their relative weight on modelled surface concentrations of the pollutants. Section 2 describes the models used and the simulations configurations. Section 3 presents the results of various simulations performed with the WRF and CHIMERE models. Section 4 presents refined results in case of the online coupling. Finally, conclusions are presented.

2 The modelling system

The two models used in this study are WRF 3.7.1, (Powers et al., 2017), and CHIMERE 2020r3, (Menut et al., 2021). The simulations are done over a single domain, with an horizontal resolution of 50 km $\times$ 50 km, as presented in Figure 2. Simulations are performed from 1^{st} July to 31^{st} August 2022. It corresponds to the same domain and the same period as presented in (Menut et al., 2023).

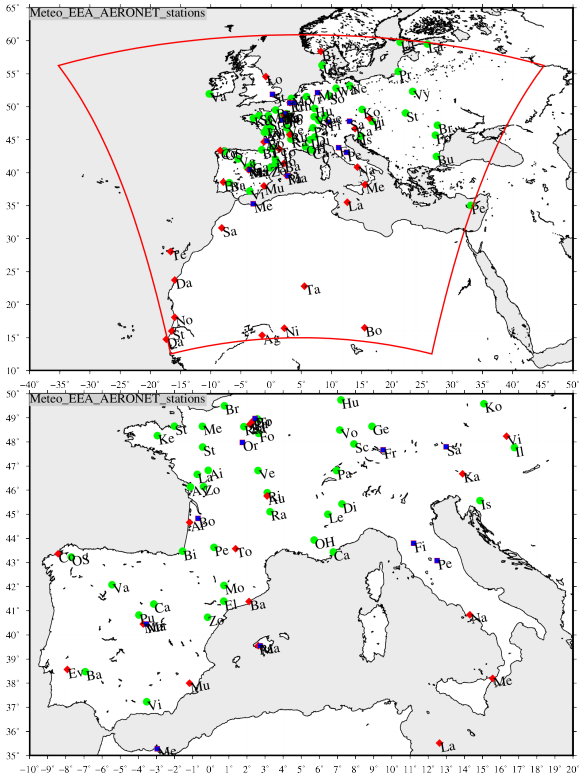

Figure 2. *Maps of measurements stations of meteorological stations (blue points), EEA (green points) and AERONET (red points). A zoom is presented over Western Europe, where stations are more numerous. For readability, only the two letters of each name is reported. The complete list of stations with their coordinates is presented in Table A1. Meteorological stations are represented with blue squares, Aeronet stations with red diamonds and pollution stations with green circles.*

The model was configured with and without spectral nudging in WRF and with and without taking into account aerosol direct and indirect effects. This leads to four different simulations as explained in Table 1.

Simulation	Nudging	Coupling	
no_nudg_offline			no nudging and offline modelling
no_nudg_online		✓	no nudging and online modelling
nudg_offline	✓		spectral nudging and offline modelling
nudg_online	✓	✓	spectral nudging and online modelling

Table 1. *Simulations performed for this study*

2.1 The WRF model set-up

2.1.1 The main schemes used

Many physical schemes are available in WRF and many studies quantified the impact of several combinations on the results, (Cohen et al., 2015). The model is used with a constant horizontal resolution of 50 km $\times$ 50 km, on an horizontal grid of 103 $\times$ 106 cells, and 28 vertical levels from the surface to 50 hPa. The Single Moment-5 class microphysics scheme is used, allowing for mixed phase processes and super cooled water (Hong et al., 2004). The radiation scheme is RRTMG scheme with the MCICA method of random cloud overlap (Mlawer et al., 1997). The surface layer scheme is based on Monin-Obukhov with Carslon-Boland viscous sub-layer. The surface physics is calculated using the Noah Land Surface Model scheme with four soil temperature and moisture layers, (Chen and Dudhia, 2001). The planetary boundary layer physics is processed using the Yonsei University scheme, (Hong et al., 2006) and the cumulus parameterization uses the ensemble scheme of (Grell and Dévényi, 2002).

2.1.2 The nudging choices

Several studies were devoted to the comparison between grid and spectral nudging, (Liu et al., 2012; Vincent and Hahmann, 2015; Ma et al., 2016; Zittis et al., 2018). The two approaches have strength and weaknesses. Grid nudging has the characteristic to be applied over all grid cells, while spectral nudging is applied only in zonal and meridional directions and only for some predefined wavenumbers. Grid nudging seems more appropriate for precipitation intensity, (Ma et al., 2016). On the other hand, spectral nudging is less intrusive at small scale and give the regional model more freedom than the large-scale forcing. One can also note that spectral nudging has a more important numerical cost than grid nudging, (Zittis et al., 2018). In this study, we prefer to use spectral nudging to have more variability at the regional scale.

Usually, the spectral nudging is applied to four meteorological variables: the wind components u and v, the temperature and the geopotential height. The nudging of specific humidity is avoided, considered as badly represented at the largest scale by the forcing model, (Heikkila et al., 2010; Otte et al., 2012). The nudging of water vapor (or moisture) is also avoided by Liu

et al. (2012), considering that this variable has no large scale features as strong as the other meteorological fields. In addition, nudging at the same time temperature and humidity may produce inconsistencies, (Sun et al., 2019). However, Spero et al. (2014) consider that not nudging this variable may be at the origin of the overestimation of precipitation when using spectral nudging, compared to grid nudging. They considered that nudging moisture guarantees to treat consistently thermodynamical fields (potential temperature and water mixing ratio). But this nudging should be restricted to below the tropopause due to too large values in the stratosphere with some global models. They also note that for moisture the best coefficient is 4.5×10^{-5} s^{-1} to be consistent with the input data fields having a 6 h frequency. Using a lower value (3×10^{-4} s^{-1}, then 1 h) induces an overprediction of precipitation. For all these studies, there is no nudging in the boundary layer.

An important parameter is the nudging coefficient (in s^{-1}), noted g. This coefficient may have different values, depending on the meteorological variable: the wind component u and v with guv, the temperature with gt and the water vapor with gq. When using spectral nudging in WRF, it is also possible to nudge geopotential height perturbations gph. With the WRF model, the default value is equal to 0.0003 s^{-1}, corresponding to a value found in many studies such as Liu et al. (2012), Otte et al. (2012), Ma et al. (2016), Gomez and Miguez-Macho (2017), Zittis et al. (2018) and Huang et al. (2021). Some others studies made sensitivity experiments to quantify the impact of this value on the results such as Choi et al. (2009), Cha et al. (2011), Glisan et al. (2013), Spero et al. (2014), He et al. (2017) and Spero et al. (2018) and no significant impact was found. This value corresponds to a one hour frequency for the nudging use and is well representative of the large scale fields used as forcing as well as to the frequency of the data used for the analysis of the global fields. In this study, this value is used for all simulations with nudging. The wind components, the potential temperature perturbation and the water vapor mixing ratio are nudged using spectral nudging with a coefficient g=0.0003 s^{-1}. There is no nudging in the Planetary Boundary Layer (PBL).

The calculation frequency is set in order to have an active nudging every time-step. The wave numbers are calculated with the hypothesis that features greater than 1000 km are sufficiently well resolved in global model, (Gomez and Miguez-Macho, 2017). Then, the following equation is applied (for example for the x direction):

$$x_{wn} = int\left(\frac{\Delta x \times N_x}{R}\right) \tag{1}$$

with Δx the horizontal resolution (in meters), N_x the number of grid cell and R the Rossby radius value, (Silva and Camargo, 2018; Mai et al., 2020). For this study and the horizontal resolution of 50 km (both in zonal and meridian directions), this leads to a wavenumber of x_{wn}=5. The same value is found for y_{wn}, having the same grid size in the two directions and a close number of cells.

2.2 The CHIMERE model configuration

This v2020r3 version of CHIMERE currently is the latest distributed one and is designed to take into account the direct and indirect effects of aerosols on cloud and radiation (the online mode) or not (the offline mode). The way these effects are taken into account is described in Briant et al. (2017) (for the direct effects) and Tuccella et al. (2019) (for the indirect effects). Mainly, the direct effect corresponds to the attenuation of radiation by aerosol layers, and the indirect effect corresponds to

cloud formation by the presence of fine particles. When used with the meteorological WRF model, CHIMERE and WRF are coupled using the OASIS-MCT coupler. As in offline mode, WRF send hourly meteorological fields for chemistry-transport to CHIMERE and CHIMERE send aerosols and Aerosol Optical Depth fields to WRF for the radiation attenuation and the microphysics in WRF.

The model configuration is exactly the same than in Menut et al. (2023): it includes emissions from anthropogenic, biogenic, sea-salt, biomass burning, lightning NO_x and mineral dust sources. It also includes gaseous and aerosol chemistry for tens of chemical species. For gases, the MELCHIOR 2 scheme is used as described in Menut et al. (2013) and Mailler et al. (2017). For aerosols, ten bins are used from 0.01 to 40 μm. Emissions include several contributions such as anthropogenic, biogenic, sea-salt, dimethylsulfide, biomass burning, lightning NO_x and mineral dust. The anthropogenic emissions are those of CAMS, (Granier et al., 2019). The dry deposition is modelled following the Zhang et al. (2001) scheme and the wet deposition following Wang et al. (2014). The biomass burning emissions are those of CAMS as described in (Kaiser et al., 2012) and with the additional term of burned area as presented in (Menut et al., 2022) and (Menut et al., 2023) and designed to calculate the impact of fires on additional mineral dust emissions, change of LAI (Leaf Area Index) and biogenic emissions. The mineral dust emissions are parameterized following (Alfaro and Gomes, 2001) and modified following (Menut et al., 2005). Vertical fluxes of emission is calculated such as the size distribution of the emission depends on the magnitude of the friction velocity, the soil distribution and its mineral characteristics. The humidity is taken into account via the soil moisture with the Fecan et al. (1999) parameterization. Precipitation and soil recovery for emission is also taken into account following (Mailler et al., 2017).

2.3 The measurements data

For the surface pollutant concentrations, the European Environment Agency (EEA, https://www.eea.europa.eu) provides a full set of hourly data for particulate matter $PM_{2.5}$, PM_{10}, ozone (O_3) and nitrogen dioxide (NO_2) for a large number of stations in Western Europe. Only urban, rural and suburban background stations are used in this study considering that the industrial and traffic ones have an inadequate spatial representativity for the present model outputs. For the Aerosol Optical Depth (AOD) and the Angström exponent (ANG), the *AErosol RObotic NETwork* (AERONET, https://aeronet.gsfc.nasa.gov/) level 1.5 measurements are used, (Holben et al., 2001). The AOD at a wavelength of λ=675 nm is daily averaged and compared to daily averaged modelled values. The available measurements values are averaged over a 24-hour period, from midnight to midnight. Only the corresponding values are considered with the model. For 2m temperature and 10m wind speed, the measurements are provided by the Weather Information website of the University of Wyoming (UWYO) (http://www.weather.uwyo.edu/). Data are provided as integer values, restraining the accuracy of the comparison to the model results. The complete list of the measurements stations is displayed in Table A1. Maps of the stations for which the measurements were used are presented in Figure 2.

The results will be presented in two different formats: general statistics to show the trend of impacts on simulated values, and examples of time-series and maps to illustrate these statistics more precisely. The measurements stations chosen as examples

are selected for their representativeness in relation to the other stations, as well as for their geographical position in relation to the processes studied.

3 Results

3.1 Statistical scores

For meteorological variables such as 2m temperature (^{o}C) and 10m wind speed (m.s^{-1}), measured by surface stations, statistical scores are presented in Table 2. These scores are calculated using all hourly data of the meteorological stations. They are defined as follows.

The variables O_t and M_t stand for the observed and modeled values, respectively, at time t. The mean value $\overline{X_N}$ is defined as:

$$\overline{X_N} = \frac{1}{N}\sum_{t=1}^{N} X_t \tag{2}$$

with N the total number of hours of the simulation. To quantify the temporal variability, the Pearson product moment correlation coefficient R is calculated as:

$$R = \frac{\frac{1}{N}\sum_{t=1}^{N}(M_t - \overline{M_t}) \times (O_t - \overline{O_t})}{\sqrt{\frac{1}{N}\sum_{t=1}^{N}(M_t - \overline{M_t})^2 \times \frac{1}{N}\sum_{t=1}^{N}(O_t - \overline{O_t})^2}}, \tag{3}$$

The spatial correlation, noted R_s, uses the same formula type except it is calculated from the temporal mean averaged values of observations and model for each location where observations are available.

$$R_s = \frac{\sum_{i=1}^{I}(\overline{M_i} - \overline{\overline{M}})\,(\overline{O_i} - \overline{\overline{O}})}{\sqrt{\sum_{i=1}^{I}(\overline{M_i} - \overline{\overline{M}})^2 \sum_{i=1}^{I}(\overline{O_i} - \overline{\overline{O}})^2}} \tag{4}$$

where I is the number of stations. The Root Mean Square Error (RMSE), is expressed as:

$$\mathrm{RMSE} = \sqrt{\frac{1}{T}\sum_{t=1}^{T}(O_{t,i} - M_{t,i})^2} \tag{5}$$

To quantify the mean differences between the several leads, the bias is also quantified as:

$$\mathrm{bias} = \frac{1}{N}\sum_{t=1}^{N}(M_t - O_t) \tag{6}$$

For these two variables, 2m temperature (T_{2m}) and 10m wind speed (u_{10m}), the best scores are obtained for the simulations with spectral nudging, but not systematically for the simulation with the coupling. The scores reflect the spatial and temporal representativeness of the variables. Temperature at 2m is more representative of the large scale than wind speed at 10m, which is more local. Given the resolution of the model, the wind scores are logically lower. Globally, it is noticeable that for meteorological variables, the nudging configurations have always better statistical scores, logically these variables being direcrly nudged. The offline configuration gives the best results, even if differences between online and offline are low.

Simulation	R_s	R_t	RMSE	bias
T_{2m}				
no_nudg_offline	0.91	0.72	2.70	-1.47
no_nudg_online	0.92	0.71	2.76	-1.60
nudg_offline	0.93	0.77	2.21	-1.24
nudg_online	0.93	0.78	2.27	-1.34
u_{10m}				
no_nudg_offline	0.29	0.45	1.23	0.63
no_nudg_online	0.25	0.48	1.23	0.62
nudg_offline	0.38	0.57	1.03	0.48
nudg_online	0.38	0.55	1.07	0.52

Table 2. *Statistical scores for 2m temperature (K) and 10m wind speed ($m.s^{-1}$). Scores are calculated for all stations and over the entire modelled period (July and August 2022). The best scores values are framed.*

For surface concentrations and optical properties, results are presented in Table 3 as statistical scores in order to quantify the relative impact of the coupling and of the spectral nudging. These scores are calculated by comparison between the modelled outputs and the measured surface concentrations and optical properties, for the corresponding location and hour.

For the surface concentrations, the three modelled chemical concentrations (ozone, $PM_{2.5}$ and PM_{10}) are compared against measurements. The spatial correlation is always the same or better when the nudging is used. In case of nudging, the spatial correlation is more or less the same for the simulation with or without coupling. For the temporal correlation, the same type of result is observed: statistical scores are systematically better with the nudging. The impact of the coupling is less important and the scores are lower with and without the coupling. The RMSE is systematically lower with the nudging as well as the bias, for the three variables.

For the optical properties, the conclusion is close as for the surface concentrations. The statistical scores are systematically better with the nudging than without. It is true for the AOD and the Angström exponent. The spatial and temporal correlations are better and the bias and the RMSE are reduced. As for surface concentrations, there is no clear impact of the use of the coupling (with direct and indirect effects) or not on the scores. The correlations are better in case of no nudging but less good with nudging. However, the impact remains low.

Simulation	R_s	R_t	RMSE	bias
Ozone				
no_nudg_offline	0.42	0.53	20.21	-4.39
no_nudg_online	0.42	0.54	20.15	-4.99
nudg_offline	0.45	0.63	18.11	-2.51
nudg_online	0.45	0.62	18.18	-2.91
$PM_{2.5}$				
no_nudg_offline	0.12	0.40	4.18	1.35
no_nudg_online	0.10	0.41	4.30	1.46
nudg_offline	0.11	0.51	3.82	1.17
nudg_online	0.12	0.51	3.76	1.08
PM_{10}				
no_nudg_offline	0.25	0.29	9.20	-4.65
no_nudg_online	0.24	0.26	9.12	-4.70
nudg_offline	0.25	0.37	8.80	-5.39
nudg_online	0.27	0.37	8.93	-5.43
AOD				
no_nudg_offline	0.82	0.40	0.16	-0.10
no_nudg_online	0.86	0.37	0.17	-0.10
nudg_offline	0.88	0.54	0.16	-0.10
nudg_online	0.86	0.52	0.16	-0.10
Angstrom				
no_nudg_offline	0.86	0.43	0.45	-0.19
no_nudg_online	0.88	0.41	0.44	-0.17
nudg_offline	0.91	0.54	0.36	-0.09
nudg_online	0.90	0.52	0.37	-0.08

Table 3. *Statistical scores for the surface ozone, $PM_{2.5}$, PM_{10} ($\mu g.m^{-3}$) concentrations, AOD (no dim.) and Angstrom exponent (no dim.) by comparison with EEA and AERONET measurements and the four simulations. Scores are calculated for all stations and over the entire modelled period (July and August 2022). The best scores values are framed.*

The conclusion of these results is that the differences between the simulations in the case of coupling (or not) is not significant. But, the differences in the case of nudging or not are significantly different and the use of the nudging always improves the simulations scores for all variables, the spatial and temporal correlations, the bias and the RMSE.

3.2 Time series of meteorological variables

As the study is based on nudging and coupling, it is important to compare impacts of the several simulations configurations on the meteorological variables. Simulations results are compared with surface measurements from meteorological stations in Europe and Africa. A list of the stations used is displayed in Table A1. Here, we present examples for two stations in France, Orléans and Bordeaux, located close to the studied fires. Bordeaux is the closest station to the studied Landes fires and directly under the fire plume and Orléans is located at 400 km to the north-east of Bordeaux, but also under the fire plume. For these two stations in France, timeseries of daily averaged 2m temperature and 10m wind speed are presented in Figure 3. Note that this type of comparison was also made for many others stations and the results are of the same kind. For the 2m temperature, simulations results are close to the measurements during the whole period. The simulations are grouped into two sets: with and without nudging. The simulations with and without coupling being very close. In Orleans and around the 20^{th} July, one can note that lower values are correctly modelled by the 'nudging' simulations when the 'no_nudging' simulations overestimate the values. Other differences are noted during the period 10^{th} to 20^{th} August when the simulations are different, both for the temperature and the wind speed.

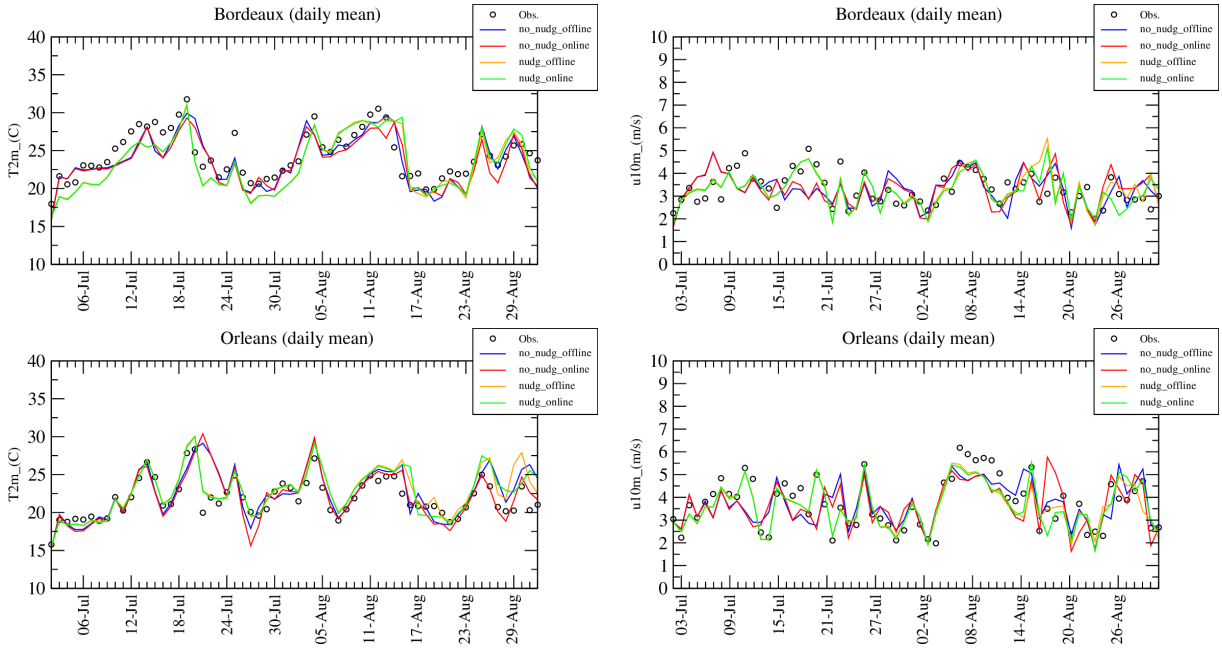

Figure 3. *Time series of daily mean 2m temperature (^oC) and 10m wind speed ($m.s^{-1}$) for the stations of Bordeaux and Orléans over the months of July and August 2022*

To better discuss these differences observed in August, a temporal zoom is done from 13^{th} to 20^{th} August and results are displayed in Figure 4. Data and model outputs are now presented at an hourly frequency. For the temperature, the first three

days show a large durnal cycle with values ranging from 18 to 40 ^{o}C, contrary to the last three days with a reduced diurnal cycle between 16 and 25 ^{o}C. The model is able to follow this weather change except around the day of 15^{th} August when the model continue to have a large diurnal cycle not observed. Except for the 15^{th} August in Bordeaux and 16^{th} August in Orleans, the four simulations provides close values of temperature. It is not the case for the 10m wind speed where all four simulations provide very different values for the six consecutive days. For example, in Orleans, the variability of the wind speed is important, ranging from 1 to 10 m.s^{-1}, depending on the simulation configuration. Finally, for the whole modelled period, there is no evidence as to which simulation best reproduces the observations, but the statistical scores (Table 2) show that the simulations with nudging performs better.

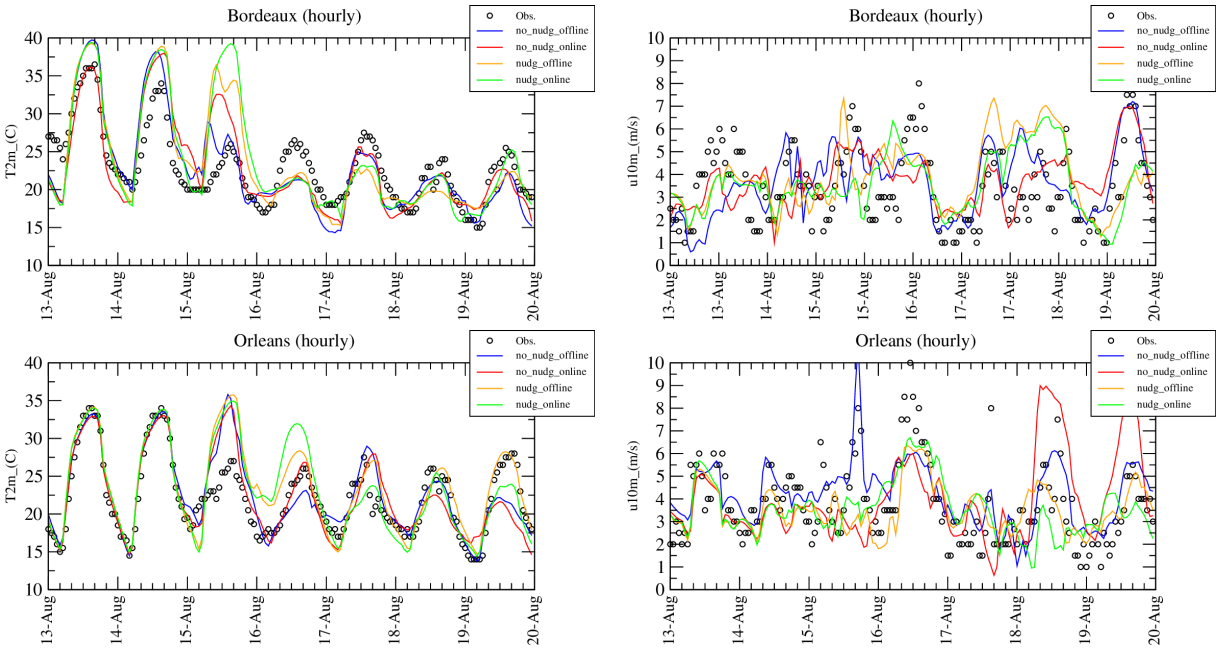

Figure 4. *Time series of hourly 2m temperature (^{o}C) and 10m wind speed (m.s^{-1}) for the stations of Bordeaux and Orléans and for the period 13 to 20 August 2022.*

3.3 Time series of surface concentrations

In order to have a more detailed look at the results, time-series of surface concentrations of ozone and $PM_{2.5}$ in μg.m^{-3}, are presented in Figure 5. Results are presented for two sites, Biarritz and Fontainebleau. As already discussed in (Menut et al., 2023), Biarritz, located in the South of France, was under the plumes of biomass burning coming from Spain mid-July and mid-August 2022. Fontainebleau, near Paris, is not close to the Landes fires but was under their plume between the 12^{th} and 18^{th} July 2022.

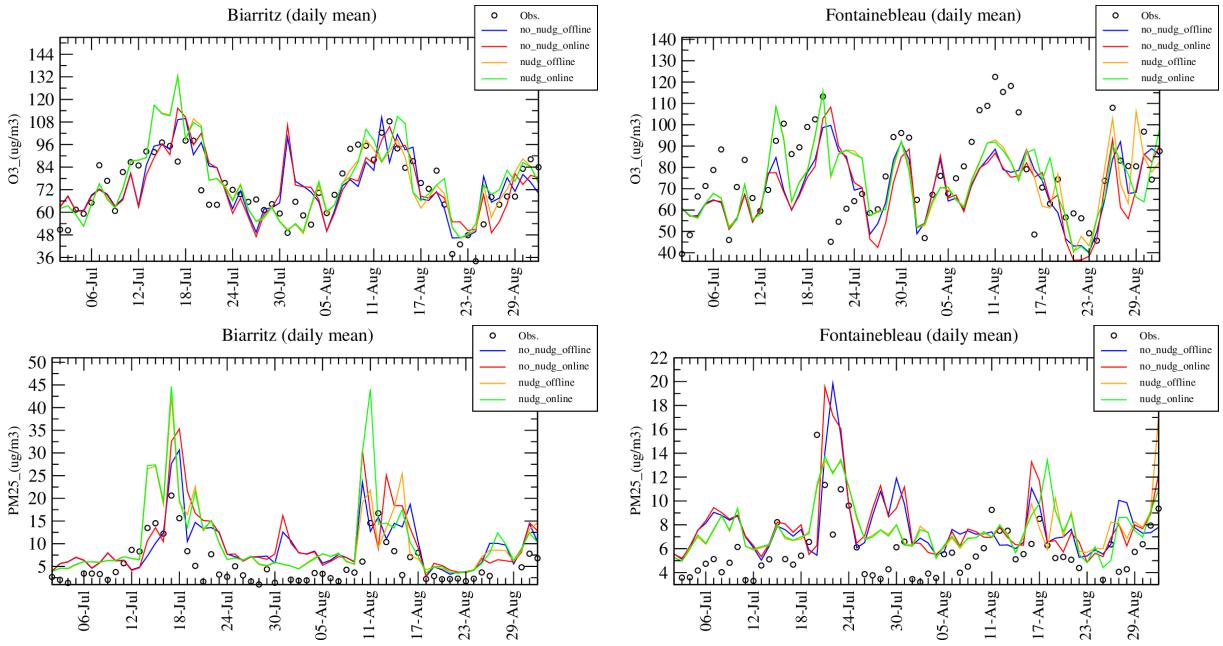

Figure 5. *Daily mean surface concentrations (in $\mu g.m^{-3}$) in Biarritz (left) and Fontainebleau (right) for ozone (O_3) and Particulate Matter with a mean mass median diameter less than 2.5 μm ($PM_{2.5}$).*

In Biarritz, two main peaks are recorded at the same time for ozone and $PM_{2.5}$: 16^{th} July and 14^{th} August 2022. For the four simulations, the magnitude and the variability of the modelled concentrations are realistic and comparable to the surface observations. It is difficult to disentangle the several simulations and to diagnose the best scores without statistical calculations. The time-series exhibits an important day to day variability for all simulations. But a third peak is modelled but not measured on July 30^{th}. It is modelled only for the configurations without nudging. With nudging, the model removes this peak and is then closer to the observations.

In Fontainebleau, the time variability is not the same between ozone and PM_{10}. But for all simulations, the model is close to the observations and the day to day variability is well reproduced. For ozone, the largest differences are for the simulation nudg_online with largest values on July 13^{th} and 19^{th}, better corresponding to the measurements. For the same simulation, and on July 21^{st}, values are lower for PM_{10} concentrations then closer to the observations than the other simulations. Note that a peak is observed for ozone around the August 13^{th} but is not modelled by any of the four simulations. This probably corresponds to long-range transport and an error in synoptic flow, and hence long-range ozone transport. This is because the configurations tested correspond to meteorological perturbations on a regional scale and within the study area. The fact that none of the four configurations simulates this peak shows that it is not due to a local or regional event.

In conclusion, the model simulations with nudging enable to avoid some non-observed peaks (such as ozone in Biarritz and PM_{10} in Fontainebleau). The four simulations have all a large day to day variability, and there is no systematic bias between

the simulations which could indicate a persistent effect of a process. The four simulations are comparable to the observations, there is no configuration being very false. It means that the use of nudging and coupling are not mutually exclusive, and that using spectral nudging, out of the boundary layer, probably does not interfere with coupling, which has more a local/regional effect.

3.4 Time series of optical depth

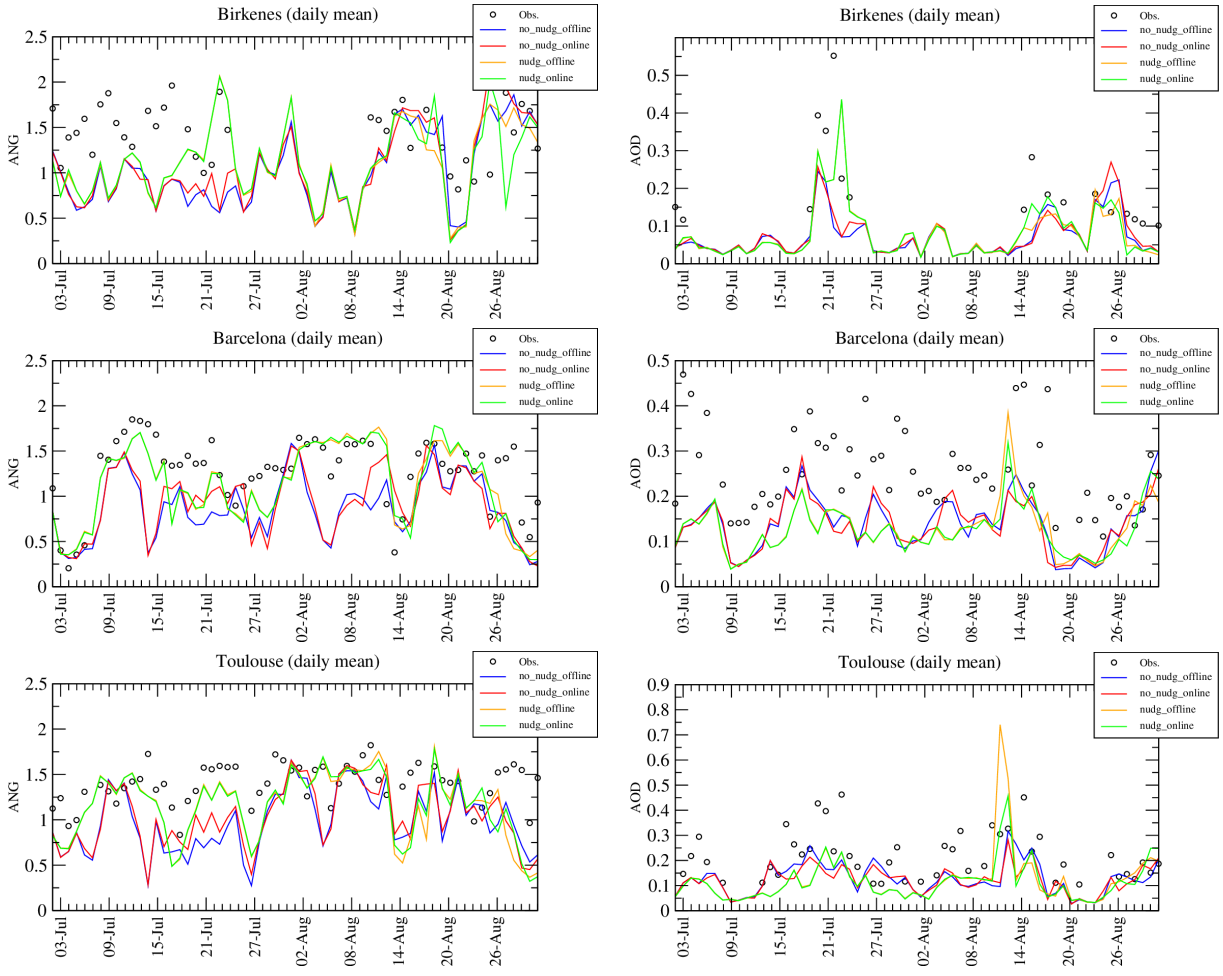

Figure 6. *Time-series of Angström exponent (ANG, left) and Aerosol Optical Depth (AOD, right) in Birkenes, Barcelona and Toulouse.*

Time-series of daily mean values are presented in Figure 6 for Angström exponent (ANG) and Aerosol Optical Depth (AOD) in Birkenes, Barcelona and Toulouse. We can expect greater differences between simulations than for surface concentrations. ANG and AOD variables incorporate changes throughout the simulated atmospheric column, the troposphere. Therefore we

take into account more possible changes between simulations, including changes on larger spatial scales such as aerosols long-range transport.

For the three sites and the two variables, one observes the same as for the surface concentrations. The two simulations with no nudging are close and the two simulations with nudging are also close. But the simulations with no nudging are very different that the simulations with nudging. This means that the direct/indirect effects are less dominant than nudging.

In Birkenes, the ANG time-series shows that the model overestimates the aerosols size by simulating coarse mode aerosols (low values of ANG) when the measurements are between 1.5 and 2 and representative of fine mode. This bias is mitigated by simulations with nudging, which better simulate the fine mode around July 21^{st}. For this day and for AOD, the simulations with nudging also better simulate an important peak with observed values around 0.5. For the rest of the period, the four simulations are relatively close, both for ANG and AOD. Birkenes being close to the desert areas where dust are emitted, the bias is reduced with the nudg-online configuration because these two forcings are able to better represent the wind speed and direction.

In Barcelona, the best capacity of the model to retrieve the observed ANG and AOD is for the simulations with nudging. It is clear for the period of July from 9^{th} to 16^{th} July when only the nudged simulations are able to simulate the high ANG values. The nudging will help the regional model to have a better wind speed. The mineral dust scheme is the one of (Alfaro and Gomes, 2001). This scheme is wind-speed dependent for the dust emission, both for the intensity of the emitted flux and for the size distribution. By changing the wind speed, the size distribution of dust is changed then for the whole amount of aerosols. The same behaviour is observed during the period from 2^{sd} to 10^{th} August when the model correctly calculated ANG around 1.5 when the non nudged simulations calculates low values (between 0.5 and 1). One can note that the simulation without nudging show non negligible differences between them. For the AOD, the four simulations underestimate the values compared to the observations. On 13^{th} August the two configurations with nudging are able to simulate an observed peak of AOD contrarily to the simulations without nudging.

In Toulouse, the ANG values are between 1 and 1.5 showing relatively small particles. The day to day variability is close to the one of Barcelona, with the same peaks at the same periods. All model configurations are close except for the period 13 to 19 July and for ANG: only the configurations with nudging are able to simulate high values of ANG close to the measurements. For AOD, also only the nudged configurations are able to reproduce a peak representative of the measurements.

In conclusion, simulations with nudging give consistently better results, especially when ANG or AOD peaks are observed. Differences can be seen between simulations without nudging and those with or without coupling. For simulations with nudging, there are no real differences for simulations with or without coupling. So we can see that nudging gives better scores but leaves less variability than for the online configurations.

3.5 Time-averaged maps

Time-averaged maps are presented in this section. The averaged period is one month from 1^{st} to 31^{st} August 2022. Then, differences are calculated between these averaged maps. Having four different configurations, the following differences are calculated:

- (nonudg_online-nonudg_offline): impact of the coupling in case of no spectral nudging
- (nudg_online-nudg_offline): impact of the coupling in case of spectral nudging
- (nudg_offline-nonudg_offline): impact of the nudging with no direct/indirect effects
- (nudg_online-nonudg_online): impact of the nudging with direct/indirect effects

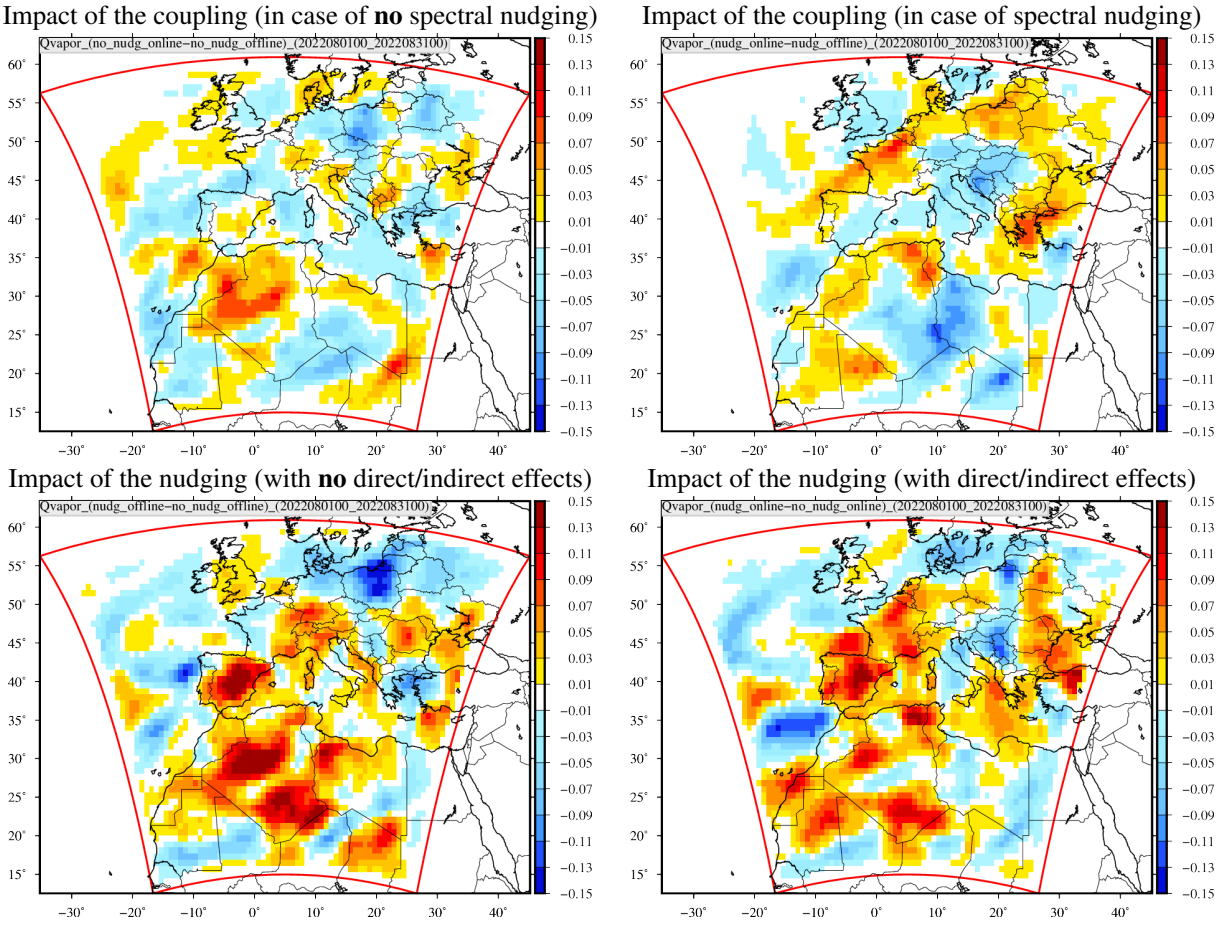

Figure 7. *Differences of vertically averaged water vapor mixing ratio (g/kg), time averaged over the period 1^{st}:31^{st} August 2022.*

Results are presented in Figure 7 for the water vapor mixing ratio, this variable is particularly important for the radiative transfer specifically at night. Water vapor as a radiative forcer contributes significantly to the greenhouse effect, between 35% and 65% for clear sky conditions and between 65% and 85% for a cloudy day as reported in (Bessagnet et al., 2020) and reference there in. The water vapor concentration fluctuates regionally and locally as shown particularly in the land/water transition bands and in mountainous areas. In these later regions, at night the long-wave radiation is one of the most important variable governing the radiative budget, a change of water mixing ratio initiated in the bottom of valleys by small motions immediately modifies the radiative balance. First of all, we note that the spatial structures of the difference values differ

between the four figures. The top figures show the impact of coupling, while the bottom figures show the impact of nudging. Depending on the location, the differences may be negative or positive. Large spatial structures exist showing that changes may affect large areas or may be transported. There is no systematic location for the negative or positive changes. The impact of the coupling is less important than the impact of nudging. The spatial structures are negative or positive and are not linked to vegetation or mountainous areas or urbanized areas. The positive changes are more important than the negatives ones.

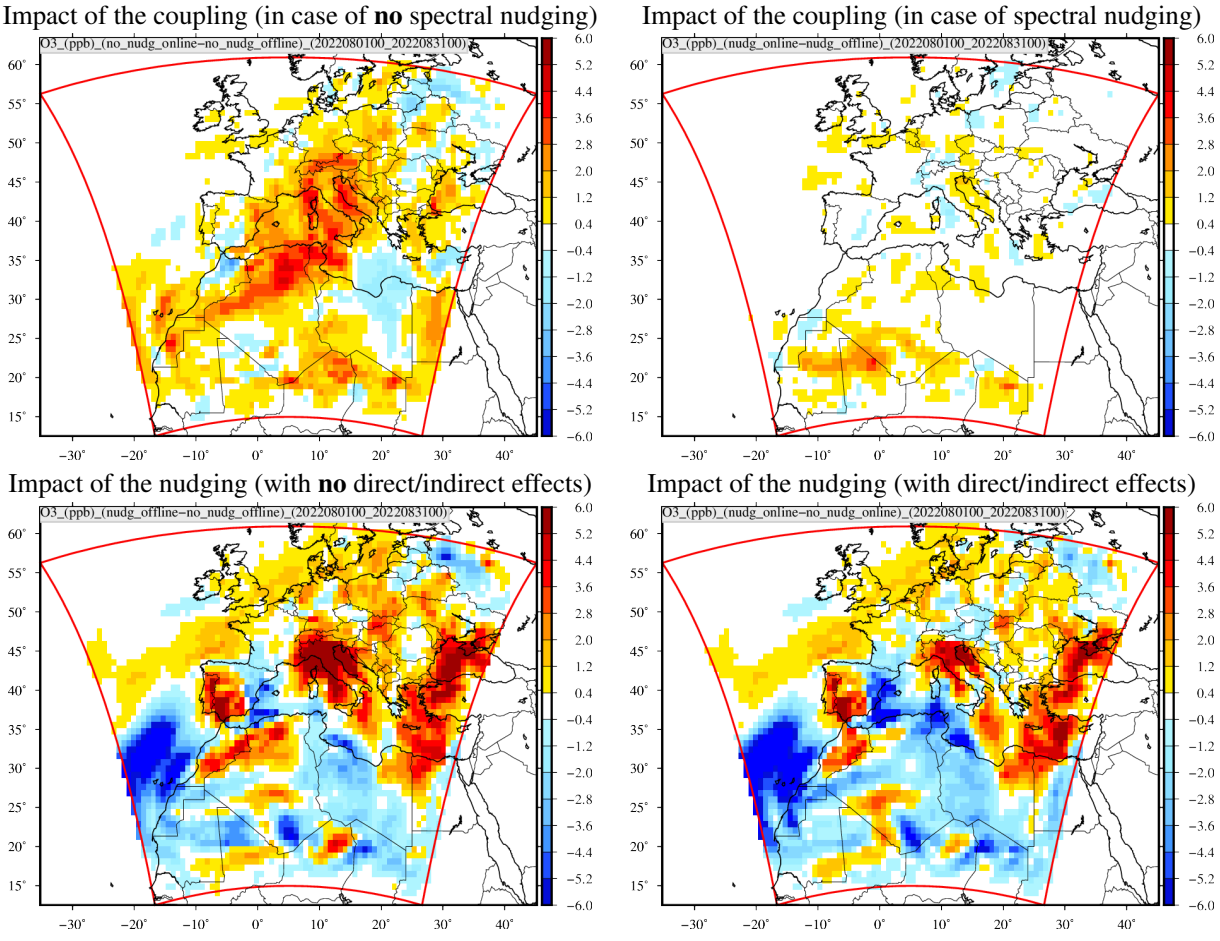

Figure 8. *Differences of surface ozone concentrations, time averaged over the period 1^{st}:31^{st} August 2022.*

The same difference calculations are done for surface ozone concentrations, Figure 8. As for the water vapor, the differences are more significant for the impact of the nudging. The spatial structure are not directly comparable between the two variables. This is normal, as we are representing a surface quantity only, which is a secondary pollutant, potentially produced and transported in a completely different way to water vapor (presented vertically integrated). For the effects of the coupling, the differences are more significant and positive over North Africa with a maximum of +3 μg.m^{-3}. Over Western Europe the differences alternate between negative and positive values, but never exceed $\pm$ 1 μg.m^{-3}. The non-zero differences are spatially

very limited and the majority of the differences are below the low value of $\pm$ 0.4 μg.m^{-3}. Figure 8 for nudg_online also shows much larger differences over the whole simulation domain. Positive and negative differences can be over sea or over land, no specific patterns are visible. Depending on the location and averaged over a month, the differences due to nudging can reach $\pm$ 6 μg.m^{-3} for surface ozone concentrations.

The previous results are summarized in Figure 9 as distributions of the values displayed in the previous maps. The comparison of all differences as distributions enables to see the spread of these differences over the domain. For all variables, the peak of the distribution is for the differences (nudg_online-nudg_offline, the green curve) and (nonudg_online-nonudg_offline, the red curve). These curves correspond to the simulations of the variability due to the coupling. The peaks indicate that these model configurations are those with the smallest differences. In addition, one can see that the differences are smaller with the green curve (nudging) than the red curve (no nudging). It means that the nudging reduces the variability of the simulations when comparing with or without coupling. The two other types of differences expressed the sensitivity of the model results to the nudging with (nudg_offline-nonudg_offline, blue curve) and (nudg_online-nonudg_online, orange curve). In this case, the peak representing the small differences is reduced and numerous large differences are calculated, both negative and positive. It means that independently of the coupling, the nudging causes many more differences than the coupling. This is the case for meteorological variables and surface pollutant concentrations.

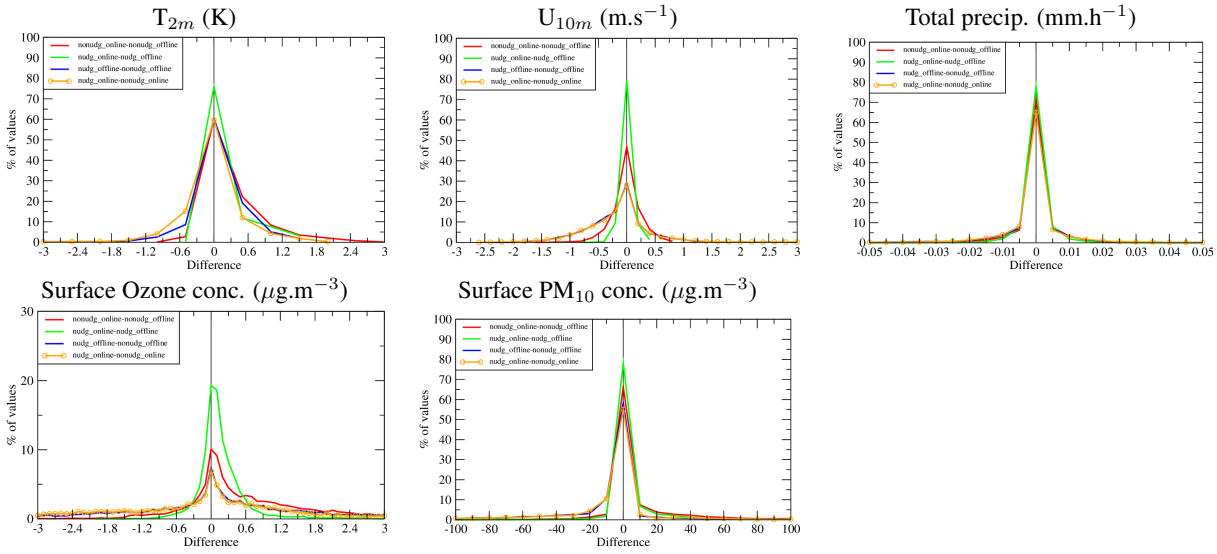

Figure 9. *Histogram of differences values, time averaged over the period 1st:31st August 2022.*

Additionally, results are also synthetized as mean averaged differences extracted from the maps of differences presented in the previous Figures. Results are in Table 4 and the goal is to try to extract an information about the variability of the coupling in case of nudging or not. The time-series and the distributions previously showed that the differences between the simulations offline and online are larger when there is no nudging than when there is nudging. The values in this Table are here to quantify

it. The mean differences are first calculated using the sign values. But as the distributions showed that there is a large variability between negative and positive differences over the entire domain, we also add the mean differences calculated using absolute values of differences.

For each variable, it is interesting to compare the two lines: in each case, the difference is between offline and online simulation, and for the case of no nudging and the case of nudging. For all variable, the differences with no nudging are larger than the differences with nudging. It is observed both for the simple differences or the differences calculated with the absolute values. It means that the nudging reduces the variability of the simulations when they are online compared to those offline.

Simulation	mean bias	mean abs(bias)
O_3		
nonudg(on-off)	0.614	0.859
nudg(on-off)	0.172	0.286
PM_{10}		
nonudg(on-off)	18.056	22.079
nudg(on-off)	8.530	10.214
T_{2m}		
nonudg(on-off)	0.299	0.356
nudg(on-off)	0.195	0.239
U_{10m}		
nonudg(on-off)	-0.005	0.170
nudg(on-off)	0.003	0.064
Precipitation		
nonudg(on-off)	-0.468	4.161
nudg(on-off)	0.101	1.815

Table 4. *Mean differences calculated with the values over the whole domain and corresponding to the mean averaged differences during the entire month of August 2022. Mean differences are calculated with the signed values and with the absolute values in order to avoid the effect of the negative/positive values, possibly reducing the mean average.*

3.6 Vertical cross-sections

Another point of view for the meteorological variables is displayed in Figure 10 with temperature vertical cross-sections. Values are displayed along the latitude (from 15 to 55 ^{o}N) and for the iso-longitude value of 5 ^{o}E. This longitude correspond to the middle of the France and the place where the fire plumes passed over the Landes (where emissions were) and then Belgium and Germany (after transport). Data are time-averaged between 10 August 00:00 UTC and 12 August 00:00 UTC. For the impact of the coupling, changes are more important in case of no spectral nudging. The largest differences are between 5000 and 8000 m with changes approximatively between $\pm$1.5 ^{o}C. For the impact of the nudging, changes are much more important

but are similar with or without the online effects. The changes are not located at the same place that for the impact of the coupling: negative values are found of ≈ -1.8 ^{o}C when they were positive in the other case. Large positive values are in the boundary layer and in the free troposphere.

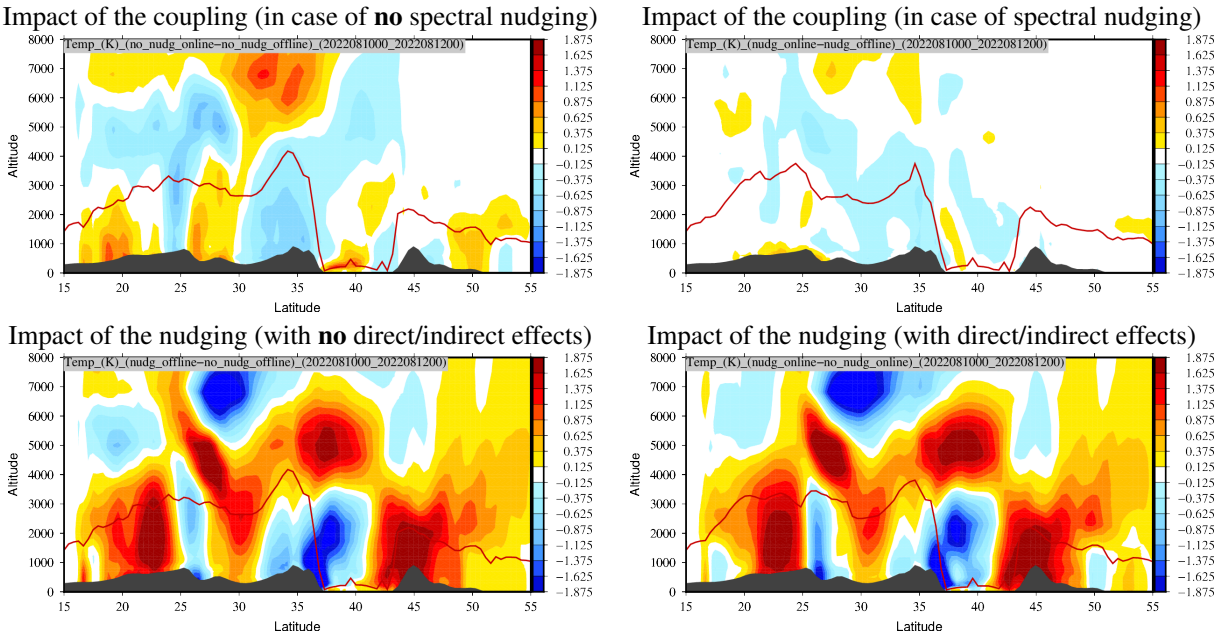

Figure 10. *Vertical cross-section of differences of temperature (^{o}C) between spectral nudging or not, coupling or not, and time averaged over the period 10st:12st August 2022. The red line represents the boundary layer height (m) of the simulation (a) if the difference is (a)-(b).*

Vertical cross-sections at a constant longitude of ozone concentrations are displayed in Figure 11 (same place and period than in the previous Figure). As for the temperature, changes are more important in case of the impact of the nudging than in case of the impact of the coupling. Changes are mostly above the boundary layer and both negative and positive with an amplitude of $\pm$ 20 μg.m^{-3}. The vertical structures are different than for temperature, not showing a direct link between the two variables. The lowest changes are in case of coupling and spectral nudging, the most realistic configuration, when ozone varies less than $\pm$ 10 μg.m^{-3} in the whole modelled atmospheric column, with very low values close to the surface.

The vertical cross-sections are also presented for PM_{10} concentrations in Figure 12. Differences are less important between the four configurations than for the previous studied variables. The largest differences are still for the impact of the nudging. Absolute differences are limited to the boundary layer, with maximum difference values of $\pm$ 300 μg.m^{-3}. The location shows these differences are mainly for latitude lower than 30 ^{o}N, indicating desert areas, then differences driven by mineral dust concentrations. In altitude, between 1000 and 3000 m, and above the Mediterranean sea (latitude 40^{o}N), negative values are found, showing that the nudging reduces the concentrations. It is collocated with an increase of ozone which can be explained by the fact that less aerosols means more radiative fluxes and therefore more photochemistry.

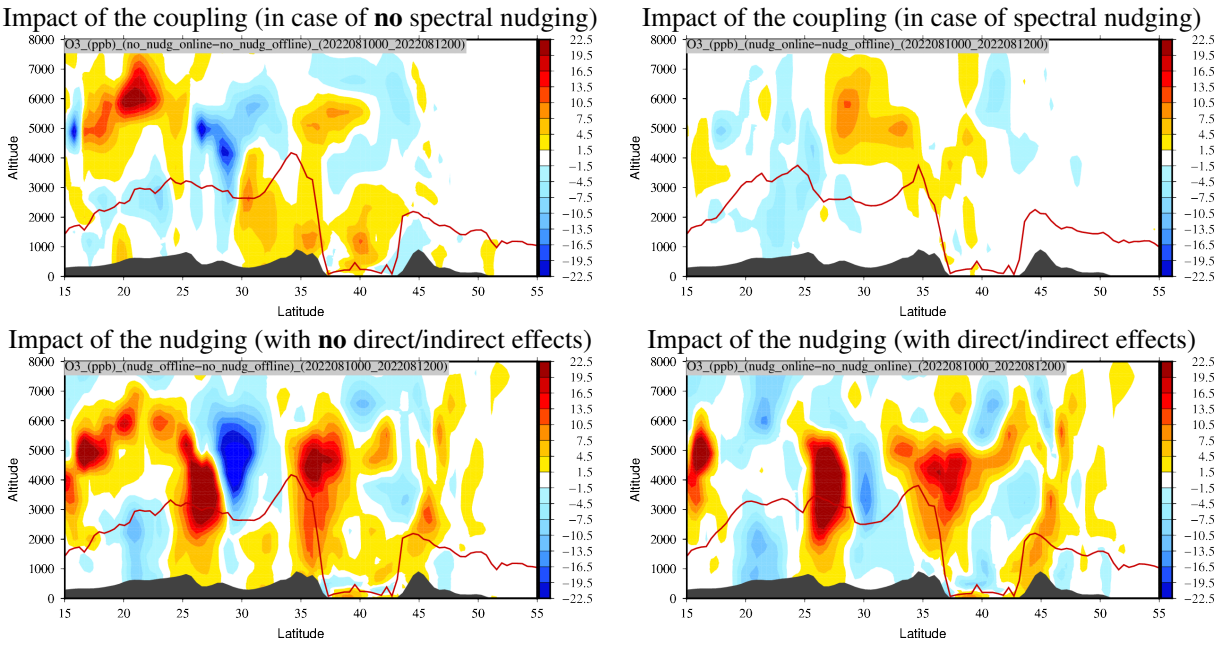

Figure 11. *Vertical cross-section of differences of O_3 ($\mu g.m^{-3}$) between spectral nudging or not, coupling or not, and time averaged over the period 10^{st}:12^{st} August 2022. The red line represents the boundary layer height (m) of the simulation (a) if the difference is (a)-(b).*

4 Online coupling: impact of the spectral nudging

It has already been shown that the impact of nudging is far greater than that of online vs. offline coupling. In the following, we will therefore only present results for the online configuration, corresponding to the most realistic processes. The differences will be calculated and presented only for the fact to use the spectral nudging or not.

Results are presented in Figure 13 for the 2m-temperature (K), 10m wind speed ($m.s^{-1}$), mineral dust emissions ($g.m^{-2}.h^{-1}$) and AOD (no dim.) between spectral nudging or not, in online coupling mode, and time averaged over the period 1^{st}:31^{st} August 2022. As for the previous presented variables, there is no systematic spatial patterns or coherent structures. This effect is always due to the fact that the results are presented as an average over a month, incorporating local changes and their transport. But the important point is to assess their magnitude in terms of differences.

For temperature, the differences are both negative and positive and can reach $\pm$ 1.5 K. For the 10m wind speed, these differences are mainly negative (a reduction in wind) except over the sea, where local positive maxima can reach 2 $m.s^{-1}$. Due to the geophysics equations, there is no reason to have a direct link between temperature and wind speed at the surface when the nudging is used: the differences are not due to the geophysics, but is due to the forcing exerted by the large scale on the regional scale by two different models. For mineral dust emissions, the differences are localised where these emissions occur, i.e. mainly in North Africa. The main trend is negative differences showing that, on average, nudging tends to reduce these emissions. The differences in AOD represent a synthesis of the previous differences, this variable representing the aerosol

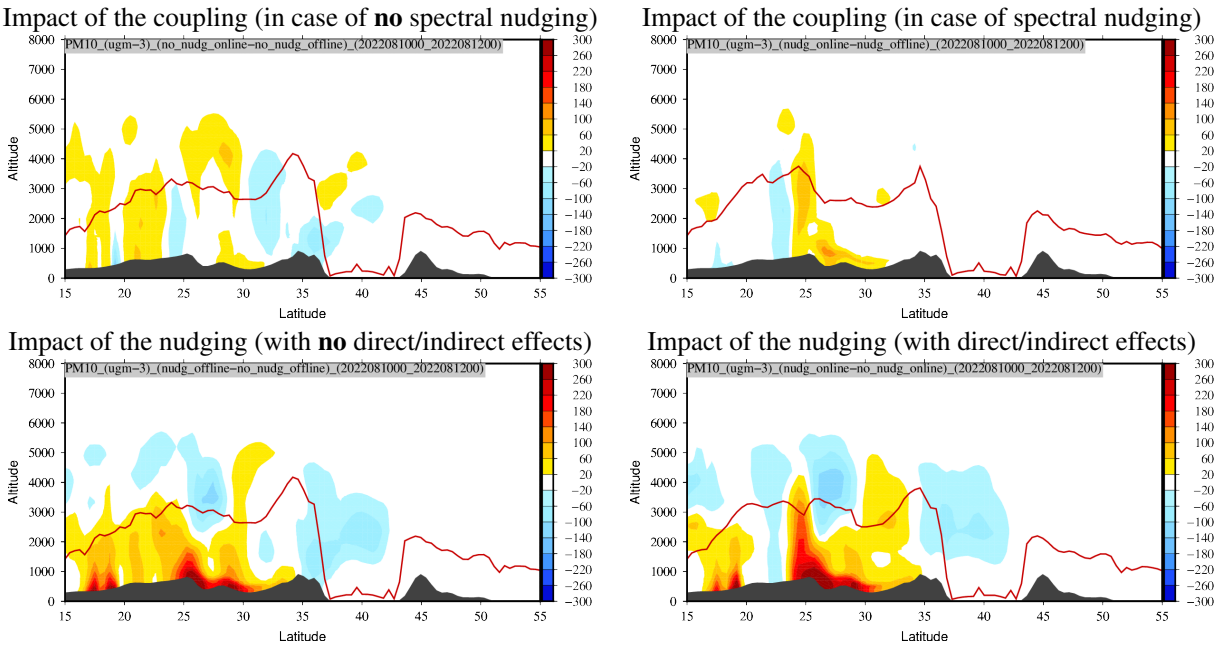

Figure 12. *Vertical cross-section of differences of PM_{10} ($\mu g.m^{-3}$) between spectral nudging or not, coupling or not, and time averaged over the period 10^{st}:12^{st} August 2022. The red line represents the boundary layer height (m) of the simulation (a) if the difference is (a)-(b).*

load in the atmosphere and therefore reflecting changes in temperature and wind speed, and therefore dust emissions, their concentrations and therefore their optical thickness. There are wide spatial variations in AOD, with large positive structures over Africa, but also large negative structures over the south-western part of the domain, including a maritime area. The differences are important and around $\pm$ 0.15. For the large area in the south-west of the domain where AOD is lower, this could be mostly due to the also negative difference in the 10m wind speed. The AOD being representative of the whole atmospheric column and the 10m wind speed only representative of the surface, the link between the differences for these two variables can't be established any further than that.

5 Conclusions

In this study, we have investigated the impact of the spectral nudging and coupling (aerosol cloud radiation) on regional simulations of atmospheric pollutants. These two processes are able to modify the meteorology, but not necessarily in the same way. Their effects can be double-counted or contraditory, however, in both cases, they should better represent the reality we try to simulate.

To quantify this impact, we carried out four simulations, each lasting two months (during the summer of 2022) and covering Europe and part of Africa. These four simulations were combinations with and without nudging and with and without coupling.

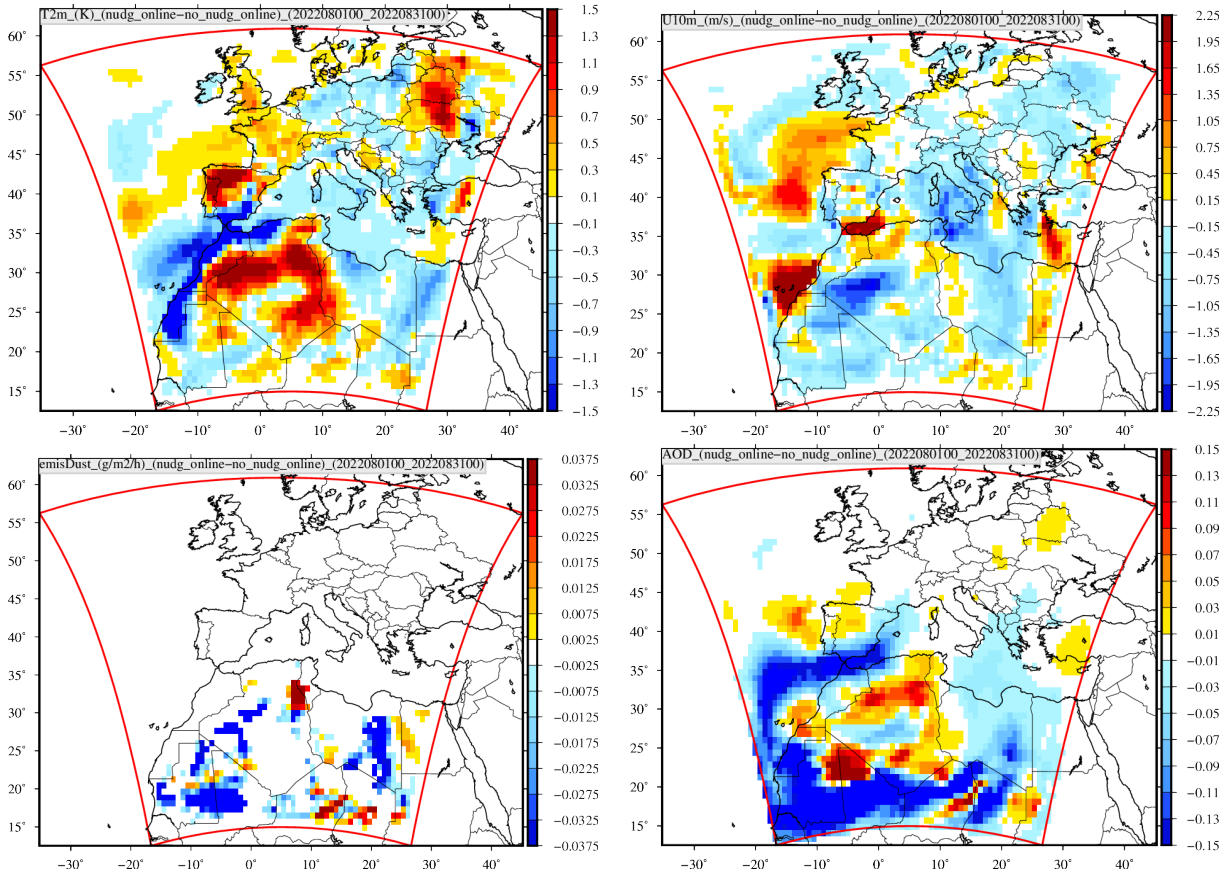

Figure 13. *Differences of 2m-temperature (K), 10m wind speed ($m.s^{-1}$), mineral dust emissions ($g.m^{-2}.h^{-1}$) and AOD (no dim.) between spectral nudging or not, in online coupling mode, and time averaged over the period from 1^{st} to 31^{st} August 2022.*

The results show first of all that the four simulations differ from one another. For the pollutants studied (O_3, PM_{10}) and for AOD, and in comparison with measurements, the simulations with nudging gives the best results, showing that, as expected, applying nudging permits to have simulation outputs closer to the observed data. At this point, the conclusions of the present study align with what is already known for climate models and extends it to chemistry-transport modelling.

We have also observed that the use of nudging reduces the sensitivity of the outputs on model configuration (in our case, the application of online coupling). As a consequence, the effect of coupling on the meteorological variables is smaller when nudging is applied, which was expected from previous studies (Pohl and Crétat, 2013), but also on the concentrations of gas-phase and particulate species (Table 4). In our case, the sensitivity of the model outputs to coupling is reduced by a factor ranging from 30 to 70% depending on the variables. While this might suggest that nudging could conduct to an underestimation of the model sensitivity to coupling, it has been shown in climate modelling that applying nudging also gives more significance to the simulated sensitivity by dampening the internal variability of the meteorological model.

The results of our study, summarized in Table 4 can be interpreted as ranges of sensitivity of the key variables in meteorology and chemistry-transport models to aerosol-meteorology feedback, with the sensitivity in the presence (resp. absence) of nudging giving an lower (resp. upper) boundary for the sensitivity of each variable to aerosol-meteorology feedback. The sensitivity determined in the absence of nudging includes the effect of the feedbacks themselves but also of the internal variability of the meteorological model, while the sensitivity in the presence of nudging includes essentially the effect of the feedbacks, but possibly dampened by nudging. For example, in the present study, the sensitivity of PM_{10} concentration to these feedbacks ranges between 10 and 22 μg.m^{-3}, that of ozone between 0.29 and 0.862 μg.m^{-3} , and between 0.24 and 0.36 K for 2m-temperature. This conclusion is of course limited to the models used, the simulation domain and the period studied, as well as the parameters chosen, particularly the nudging constants.

An important outcome of this study lies in the fact that the use of nudging and coupling options can have counter intuitive impacts when CTM are used to analyse the impact of emission reduction scenarios. For instance, it is very important to keep in mind that in the case of a meteorological online system, concentrations change not only because emissions change but also because of feedbacks of aerosols on meteorology. As a perspective of this study, simulations should be repeated with nested domains to address one other dimension of the problem: the impact of the horizontal resolution.

Code availability. The CHIMERE v2020 model is available on its dedicated web site https://www.lmd.polytechnique.fr and for download at https://doi.org/10.14768/8afd9058-909c-4827-94b8-69f05f7bb46d.

Data availability. All data used in this study, as well as the data required to run the simulations, are available on the CHIMERE web site download page https://doi.org/10.14768/8afd9058-909c-4827-94b8-69f05f7bb46d.

Author contributions. All authors contributed to the model development. LM coordinated the manuscript and all authors wrote a part and reviewed it.

Competing interests. The authors declare that they have no conflict of interest.

Acknowledgements. The authors thank the OASIS modeling team for their support with the OASIS coupler, the WRF developers team for the free use of their model. We thank the investigators and staff who maintain and provide the AERONET data (https://aeronet.gsfc.nasa.gov/). European Environmental Agency (EEA) is acknowledged for their air quality station data that is provided and freely downloadable (https://www.eea.europa.eu/data-and-maps/data/aqereporting-8).

References

Alfaro, S. C. and Gomes, L.: Modeling mineral aerosol production by wind erosion: Emission intensities and aerosol size distribution in source areas, J. Geophys. Res., 106, 18,075–18,084, 2001.

Berthou, S., Mailler, S., Drobinski, P., Arsouze, T., Bastin, S., Béranger, K., and Brossier, C. L.: Lagged effects of the Mistral wind on heavy precipitation through ocean-atmosphere coupling in the region of Valencia (Spain), Climate Dynamics, 51, 969–983, https://doi.org/10.1007/s00382-016-3153-0, 2016.

Bessagnet, B., Menut, L., Lapere, R., Couvidat, F., Jaffrezo, J.-L., Mailler, S., Favez, O., Pennel, R., and Siour, G.: High Resolution Chemistry Transport Modeling with the On-Line CHIMERE-WRF Model over the French Alps-Analysis of a Feedback of Surface Particulate Matter Concentrations on Mountainous Meteorology, Atmosphere, 11, https://doi.org/10.3390/atmos11060565, 2020.

Briant, R., Tuccella, P., Deroubaix, A., Khvorostyanov, D., Menut, L., Mailler, S., and Turquety, S.: Aerosol–radiation interaction modelling using online coupling between the WRF 3.7.1 meteorological model and the CHIMERE 2016 chemistry-transport model, through the OASIS3-MCT coupler, Geoscientific Model Development, 10, 927–944, https://doi.org/10.5194/gmd-10-927-2017, 2017.

Cha, D.-H., Jin, C.-S., Lee, D.-K., and Kuo, Y.-H.: Impact of intermittent spectral nudging on regional climate simulation using Weather Research and Forecasting model, Journal of Geophysical Research: Atmospheres, 116, https://doi.org/https://doi.org/10.1029/2010JD015069, 2011.

Chen, F. and Dudhia, J.: Coupling an advanced land surface-hydrology model with the Penn State-NCAR MM5 modeling system. Part I: Model implementation and sensitivity, Mon. Weather Rev., 129(4), 569–585, 2001.

Choi, H.-J., Lee, H. W., Sung, K.-H., Kim, M.-J., Kim, Y.-K., and Jung, W.-S.: The impact of nudging coefficient for the initialization on the atmospheric flow field and the photochemical ozone concentration of Seoul, Korea, Atmospheric Environment, 43, 4124–4136, https://doi.org/https://doi.org/10.1016/j.atmosenv.2009.05.051, 2009.

Cohen, A. E., Cavallo, S. M., Coniglio, M. C., and Brooks, H. E.: A Review of Planetary Boundary Layer Parameterization Schemes and Their Sensitivity in Simulating Southeastern U.S. Cold Season Severe Weather Environments, Weather and Forecasting, 30, 591–612, https://doi.org/10.1175/WAF-D-14-00105.1, 2015.

Fecan, F., Marticorena, B., and Bergametti, G.: Parameterization of the increase of aeolian erosion threshold wind friction velocity due to soil moisture for arid and semi-arid areas, Annals of Geophysics, 17, 149–157, 1999.

Glisan, J. M., Gutowski, W. J., Cassano, J. J., and Higgins, M. E.: Effects of Spectral Nudging in WRF on Arctic Temperature and Precipitation Simulations, Journal of Climate, 26, 3985 – 3999, https://doi.org/https://doi.org/10.1175/JCLI-D-12-00318.1, 2013.

Gomez, B. and Miguez-Macho, G.: The impact of wave number selection and spin-up time in spectral nudging, Quarterly Journal of the Royal Meteorological Society, 143, 1772–1786, https://doi.org/https://doi.org/10.1002/qj.3032, 2017.

Granier, C., Darras, S., van der Gon, H. D., Doubalova, J., Elguindi, N., Galle, B., Gauss, M., Guevara, M., Jalkanen, J.-P., Kuenen, J., Liousse, C., Quack, B., Simpson, D., and Sindelarova, K.: The Copernicus Atmosphere Monitoring Service global and regional emissions (April 2019 version), Tech. rep., ECMWF, https://doi.org/10.24380/d0bn-kx16, copernicus Atmosphere Monitoring Service, 2019.

Grell, G. and Dévényi, D.: A generalized approach to parameterizing convection combining ensemble and data assimilation techniques, Geophysical Research Letters, 29, 38–1–38–4, https://doi.org/10.1029/2002GL015311, 2002.

He, J., Glotfelty, T., Yahya, K., Alapaty, K., and Yu, S.: Does temperature nudging overwhelm aerosol radiative effects in regional integrated climate models?, Atmospheric Environment, 154, 42–52, https://doi.org/https://doi.org/10.1016/j.atmosenv.2017.01.040, 2017.

Heikkila, U., Sandvik, A., and Sorteberg, A.: Dynamical downscaling of ERA-40 in complex terrain using the WRF regional climate model, Climate Dynamics, 37, 1551–1564, https://doi.org/10.1007/s00382-010-0928-6, 2010.

Hogrefe, C., Pouliot, G., Wong, D., Torian, A., Roselle, S., Pleim, J., and Mathur, R.: Annual application and evaluation of the online coupled WRF-CMAQ system over North America under AQMEII phase 2, Atmospheric Environment, 115, 683–694, https://doi.org/https://doi.org/10.1016/j.atmosenv.2014.12.034, 2015.

Holben, B., Tanre, D., Smirnov, A., Eck, T. F., Slutsker, I., Abuhassan, N., Newcomb, W. W., Schafer, J., Chatenet, B., Lavenu, F., Kaufman, Y. J., Vande Castle, J., Setzer, A., Markham, B., Clark, D., Frouin, R., Halthore, R., Karnieli, A., O'Neill, N. T., Pietras, C., Pinker, R. T., Voss, K., and Zibordi, G.: An emerging ground-based aerosol climatology: Aerosol Optical Depth from AERONET, J. Geophys. Res., 106, 12 067–12 097, 2001.

Hong, S. Y., Dudhia, J., and Chen, S.: A revised approach to ice microphysical processes for the bulk parameterization of clouds and precipitation, Mon. Weather Rev., 132, 103–120, 2004.

Hong, S. Y., Noh, Y., and Dudhia, J.: A new vertical diffusion package with an explicit treatment of entrainment processes, Mon. Weather Rev., 134, 2318–2341, https://doi.org/10.1175/MWR3199.1, 2006.

Huang, Z., Zhong, L., Ma, Y., and Fu, Y.: Development and evaluation of spectral nudging strategy for the simulation of summer precipitation over the Tibetan Plateau using WRF (v4.0), Geoscientific Model Development, 14, 2827–2841, https://doi.org/10.5194/gmd-14-2827-2021, 2021.

Kaiser, J. W., Heil, A., Andreae, M. O., Benedetti, A., Chubarova, N., Jones, L., Morcrette, J.-J., Razinger, M., Schultz, M. G., Suttie, M., and van der Werf, G. R.: Biomass burning emissions estimated with a global fire assimilation system based on observed fire radiative power, Biogeosciences, 9, 527–554, https://doi.org/10.5194/bg-9-527-2012, 2012.

Kooperman, G. J., Pritchard, M. S., Ghan, S. J., Wang, M., Somerville, R. C. J., and Russell, L. M.: Constraining the influence of natural variability to improve estimates of global aerosol indirect effects in a nudged version of the Community Atmosphere Model 5, Journal of Geophysical Research: Atmospheres, 117, n/a–n/a, https://doi.org/10.1029/2012jd018588, 2012.

Kruse, C. G., Bacmeister, J. T., Zarzycki, C. M., Larson, V. E., and Thayer-Calder, K.: Do Nudging Tendencies Depend on the Nudging Timescale Chosen in Atmospheric Models?, Journal of Advances in Modeling Earth Systems, 14, e2022MS003 024, https://doi.org/https://doi.org/10.1029/2022MS003024, e2022MS003024 2022MS003024, 2022.

Lin, G., Wan, H., Zhang, K., Qian, Y., and Ghan, S. J.: Can nudging be used to quantify model sensitivities in precipitation and cloud forcing?, Journal of Advances in Modeling Earth Systems, 8, 1073–1091, https://doi.org/10.1002/2016ms000659, 2016.

Liu, P., Tsimpidi, A. P., Hu, Y., Stone, B., Russell, A. G., and Nenes, A.: Differences between downscaling with spectral and grid nudging using WRF, Atmospheric Chemistry and Physics, 12, 3601–3610, https://doi.org/10.5194/acp-12-3601-2012, 2012.

Ma, Y., Yang, Y., Mai, X., Qiu, C., Long, X., and Wang, C.: Comparison of Analysis and Spectral Nudging Techniques for Dynamical Downscaling with the WRF Model over China, Advances in Meteorology, 4761513, 1687–9309, https://doi.org/10.1155/2016/4761513, 2016.

Mai, X., Qiu, X., Yang, Y., and Ma, Y.: Impacts of Spectral Nudging Parameters on Dynamical Downscaling in Summer over Mainland China, Frontiers in Earth Science, 8, https://doi.org/10.3389/feart.2020.574754, 2020.

Mailler, S., Menut, L., Khvorostyanov, D., Valari, M., Couvidat, F., Siour, G., Turquety, S., Briant, R., Tuccella, P., Bessagnet, B., Colette, A., Létinois, L., Markakis, K., and Meleux, F.: CHIMERE-2017: from urban to hemispheric chemistry-transport modeling, Geoscientific Model Development, 10, 2397–2423, https://doi.org/10.5194/gmd-10-2397-2017, 2017.

Menut, L., C.Schmechtig, and B.Marticorena: Sensitivity of the sandblasting fluxes calculations to the soil size distribution accuracy, Journal of Atmospheric and Oceanic Technology, 22, 1875–1884, 2005.

Menut, L., Bessagnet, B., Khvorostyanov, D., Beekmann, M., Blond, N., Colette, A., Coll, I., Curci, G., Foret, F., Hodzic, A., Mailler, S., Meleux, F., Monge, J., Pison, I., Siour, G., Turquety, S., Valari, M., Vautard, R., and Vivanco, M.: CHIMERE 2013: a model for regional atmospheric composition modelling, Geoscientific Model Development, 6, 981–1028, https://doi.org/10.5194/gmd-6-981-2013, 2013.

Menut, L., Bessagnet, B., Briant, R., Cholakian, A., Couvidat, F., Mailler, S., Pennel, R., Siour, G., Tuccella, P., Turquety, S., and Valari, M.: The CHIMERE v2020r1 online chemistry-transport model, Geoscientific Model Development, 14, 6781–6811, https://doi.org/10.5194/gmd-14-6781-2021, 2021.

Menut, L., Siour, G., Bessagnet, B., Cholakian, A., Pennel, R., and Mailler, S.: Impact of Wildfires on Mineral Dust Emissions in Europe, Journal of Geophysical Research: Atmospheres, 127, e2022JD037 395, https://doi.org/https://doi.org/10.1029/2022JD037395, e2022JD037395 2022JD037395, 2022.

Menut, L., Cholakian, A., Siour, G., Lapere, R., Pennel, R., Mailler, S., and Bessagnet, B.: Impact of Landes forest fires on air quality in France during the 2022 summer, Atmospheric Chemistry and Physics, 23, 7281–7296, https://doi.org/10.5194/acp-23-7281-2023, 2023.

Mlawer, E., Taubman, S., Brown, P., Iacono, M., and Clough, S.: Radiative transfer for inhomogeneous atmospheres: RRTM a validated correlated-k model for the longwave, J. Geophys. Res., 102, 16 663–16 682, 1997.

Otte, T. L., Nolte, C. G., Otte, M. J., and Bowden, J. H.: Does Nudging Squelch the Extremes in Regional Climate Modeling?, Journal of Climate, 25, 7046 – 7066, https://doi.org/https://doi.org/10.1175/JCLI-D-12-00048.1, 2012.

Pohl, B. and Crétat, J.: On the use of nudging techniques for regional climate modeling: application for tropical convection, Climate Dynamics, 43, 1693–1714, https://doi.org/10.1007/s00382-013-1994-3, 2013.

Powers, J. G., Klemp, J. B., Skamarock, W. C., Davis, C. A., Dudhia, J., Gill, D. O., Coen, J. L., Gochis, D. J., Ahmadov, R., Peckham, S. E., Grell, G. A., Michalakes, J., Trahan, S., Benjamin, S. G., Alexander, C. R., Dimego, G. J., Wang, W., Schwartz, C. S., Romine, G. S., Liu, Z., Snyder, C., Chen, F., Barlage, M. J., Yu, W., and Duda, M. G.: The Weather Research and Forecasting Model: Overview, System Efforts, and Future Directions, Bulletin of the American Meteorological Society, 98, 1717–1737, https://doi.org/10.1175/BAMS-D-15-00308.1, 2017.

Rizza, U., Mancinelli, E., Canepa, E., Piazzola, J., Missamou, T., Yohia, C., Morichetti, M., Virgili, S., Passerini, G., and Miglietta, M. M.: WRF Sensitivity Analysis in Wind and Temperature Fields Simulation for the Northern Sahara and the Mediterranean Basin, Atmosphere, 11, https://doi.org/10.3390/atmos11030259, 2020.

Silva, N. P. d. and Camargo, R. d.: Impact of Wave Number Choice in Spectral Nudging Applications During a South Atlantic Convergence Zone Event, Frontiers in Earth Science, 6, https://doi.org/10.3389/feart.2018.00232, 2018.

Song, S., Tang, J., and Chen, X.: Impacts of spectral nudging on the sensitivity of a regional climate model to convective parameterizations in East Asia, Acta Meteorologica Sinica, 25, 63–77, https://doi.org/10.1007/s13351-011-0005-z, 2011.

Spero, T. L., Otte, M. J., Bowden, J. H., and Nolte, C. G.: Improving the representation of clouds, radiation, and precipitation using spectral nudging in the Weather Research and Forecasting model, Journal of Geophysical Research: Atmospheres, 119, 11,682–11,694, https://doi.org/https://doi.org/10.1002/2014JD022173, 2014.

Spero, T. L., Nolte, C. G., Mallard, M. S., and Bowden, J. H.: A Maieutic Exploration of Nudging Strategies for Regional Climate Applications Using the WRF Model, Journal of Applied Meteorology and Climatology, 57, 1883 – 1906, https://doi.org/https://doi.org/10.1175/JAMC-D-17-0360.1, 2018.

Sun, J., Zhang, K., Wan, H., Ma, P.-L., Tang, Q., and Zhang, S.: Impact of Nudging Strategy on the Climate Representativeness and Hindcast Skill of Constrained EAMv1 Simulations, Journal of Advances in Modeling Earth Systems, 11, 3911–3933, https://doi.org/10.1029/2019MS001831, 2019.

Tuccella, P., Menut, L., Briant, R., Deroubaix, A., Khvorostyanov, D., Mailler, S., Siour, G., and Turquety, S.: Implementation of Aerosol-Cloud Interaction within WRF-CHIMERE Online Coupled Model: Evaluation and Investigation of the Indirect Radiative Effect from Anthropogenic Emission Reduction on the Benelux Union, Atmosphere, 10, https://doi.org/10.3390/atmos10010020, 2019.

Vincent, C. L. and Hahmann, A. N.: The Impact of Grid and Spectral Nudging on the Variance of the Near-Surface Wind Speed, Journal of Applied Meteorology and Climatology, 54, 1021 – 1038, https://doi.org/https://doi.org/10.1175/JAMC-D-14-0047.1, 2015.

von Storch, H. and Zwiers, F.: Statistical Analysis in Climate Research, Cambridge University Press, 2001.

Wang, X., Zhang, L., and Moran, M. D.: Development of a new semi-empirical parameterization for below-cloud scavenging of size-resolved aerosol particles by both rain and snow, Geoscientific Model Development, 7, 799–819, https://doi.org/10.5194/gmd-7-799-2014, 2014.

Zhang, L., Gong, S., Padro, J., and Barrie, L.: A size-segregated particle dry deposition scheme for an atmospheric aerosol module, Atmospheric Environment, 35(3), 549–560, 2001.

Zittis, G., Bruggeman, A., Hadjinicolaou, P., Camera, C., and Lelieveld, J.: Effects of Meteorology Nudging in Regional Hydroclimatic Simulations of the Eastern Mediterranean, Atmosphere, 9, https://doi.org/10.3390/atmos9120470, 2018.

Appendix A: List of measurements stations

Site	Longitude (^{o})	Latitude (^{o})	Site	Longitude (^{o})	Latitude (^{o})	Site	Longitude (^{o})	Latitude (^{o})
Meteorological stations			Palma	2.62	39.55	Moerkerke	3.36	51.25
Madrid	-3.55	40.45	Paris	2.33	48.86	Neuglobsow	13.03	53.16
Mallorca	2.73	39.55	Saada	-8.15	31.62	OHP	5.71	43.93
Bordeaux	-0.7	44.83	Saclay	2.16	48.73	OSavinao	-7.69	43.23
Firenze	11.2	43.8	Toulouse	1.37	43.57	Payerne	6.94	46.81
Orleans	1.75	47.98	Vienna	16.33	48.23	Peyrusse	0.17	43.62
Lille	3.1	50.57	**Pollutants stations**			Peristerona	33.05	35.03
Salzburg	13.00	47.80	Aytre	-1.11	46.13	PuertoCotos	-3.96	40.82
Munster	7.70	52.13	Airvault	-0.13	46.82	Preila	21.06	55.35
Stansted	0.23	51.88	Barcarrota	-6.92	38.47	Rageade	3.27	45.10
Melilla	-2.95	35.28	Biarritz	-1.55	43.47	Rambouillet	1.83	48.63
Perugia	12.50	43.08	Burgas	27.38	42.46	Riom	3.12	45.89
Chievres	3.83	50.57	Brotonne	0.75	49.49	Starina	22.26	49.05
Bourget	2.45	48.97	Breazu	27.54	47.19	StDenisAnjou	-0.44	47.78
Friedrichshafen	9.52	47.67	Carling	6.76	43.43	StMalo	-2.00	48.65
AOD stations			Campisabalos	-3.14	41.28	Solling	9.55	51.70
Arcachon	-1.16	44.66	Diga	7.24	45.43	Schauinsland	7.90	47.91
Palaiseau	2.20	48.70	ElsTorms	0.71	41.40	Tremblay	2.57	48.95
Aubiere	3.11	45.76	Fontainebleau	2.64	48.35	Ulborg	8.43	56.28
Barcelona	2.11	41.38	Focsani	27.21	45.69	Uto	21.37	59.77
Birkenes	8.25	58.38	Germany	8.90	48.64	Valentia	-10.24	51.93
Coruna	-8.42	43.36	Hunsr	7.19	49.74	Viznar	-3.53	37.23
Evora	-7.91	38.56	Illmitz	16.76	47.76	Verneuil	2.61	46.81
Kanzelhohe	13.90	46.67	Iskrba	14.86	45.56	Valderas	-5.44	42.07
Lampedusa	12.63	35.51	Kergoff	-2.94	48.26	Vredepeel	5.85	51.54
Lille	3.14	50.61	LaTardiere	-0.74	46.65	Vosges	7.12	48.49
Loftus	-0.86	54.56	Kosetice	15.08	49.58	Vredepeel	5.85	51.54
Madrid	-3.72	40.45	LaTardiere	-0.74	46.65	Vysokoe	23.43	52.33
Murcia	-1.17	38.00	LeCasset	6.46	45.00	Waldhof	10.75	52.80
Messina	15.56	38.19	Lahemaa	25.90	59.50	Zoodyss	-0.39	46.14
Murcia	-1.17	38.00	Mera	-0.45	48.64	Zorita	-0.16	40.73
Napoli	14.30	40.83	MontsecOAM	0.72	42.05			

Table A1. *Name and location of measurements stations used in this study.*